

We are IntechOpen, the world's leading publisher of Open Access books Built by scientists, for scientists

6,500

Open access books available

176,000

International authors and editors

190M

Downloads

Our authors are among the

154

Countries delivered to

TOP 1%

most cited scientists

12.2%

Contributors from top 500 universities



WEB OF SCIENCE™

Selection of our books indexed in the Book Citation Index
in Web of Science™ Core Collection (BKCI)

Interested in publishing with us?
Contact book.department@intechopen.com

Numbers displayed above are based on latest data collected.
For more information visit www.intechopen.com



Chapter

Physical, Biological, and Clinical Merits of High Energy Boron Ions for Radiation Therapy

Anders Brahme

Abstract

The lightest ions beyond protons, principally helium, lithium, and boron ions, make highly specific molecular Bragg peak radiation therapy of malignant tumors possible with minimal adverse normal tissue reactions. The Bragg peak ionization density is mainly elevated in a few mm wide spot at the end of these ions with substantially increased local apoptosis and senescence induction. Mainly placing Bragg peaks in the gross tumor volume with increased local therapeutic effect and only low ionization density and easily repairable damage in normal tissues. The possible geometrical accuracy of the dose delivery will be ≈ 1 mm with these ions. Interestingly, high-resolution molecular tumor imaging will then be possible, particularly with ^8B boron ions that are our lightest positron emitter allowing immediate accurate PET-CT imaging to delineate the target volume dose delivery. Compared to carbon ions the boron radiation damage to normal tissues in front of and behind the tumor is reduced at the same time as tumor apoptosis and senescence are increased. A mean tumor cure as high as 80% should be possible with Boron ion therapy using new clinical fractionation principles and even more when early tumor detection and malignancy estimation methods are brought into more regular clinical use.

Keywords: boron ion radiation therapy, $^8\text{-}^{11}\text{B}$ boron ions, low dose apoptosis, low dose hypersensitivity, high dose apoptosis, radiation dose-response relationships, light ion radiation therapy, radiation therapy optimization

1. Introduction

The interaction of ionizing radiation with living tissues and tumors is one of the most complex biomedical problems, since it requires knowledge about atomic and nuclear physics and the generated secondary electrons, as well as the molecular biology dynamics of living tissues and cells and their complex damage repair systems [1]. Understanding radiation-induced cellular damage and repair is the key to optimal safety in the therapeutic and the diagnostic use of high-quality radiation beams. Biologically optimized intensity-modulated photons, electrons, and light ions represent the ultimate development of radiation therapy as shown in **Figure 1**. The absorbed dose and biological effect on normal tissues can be designed so it is as low as possible from a radiation physical point of view, at the same time, as the therapeutic

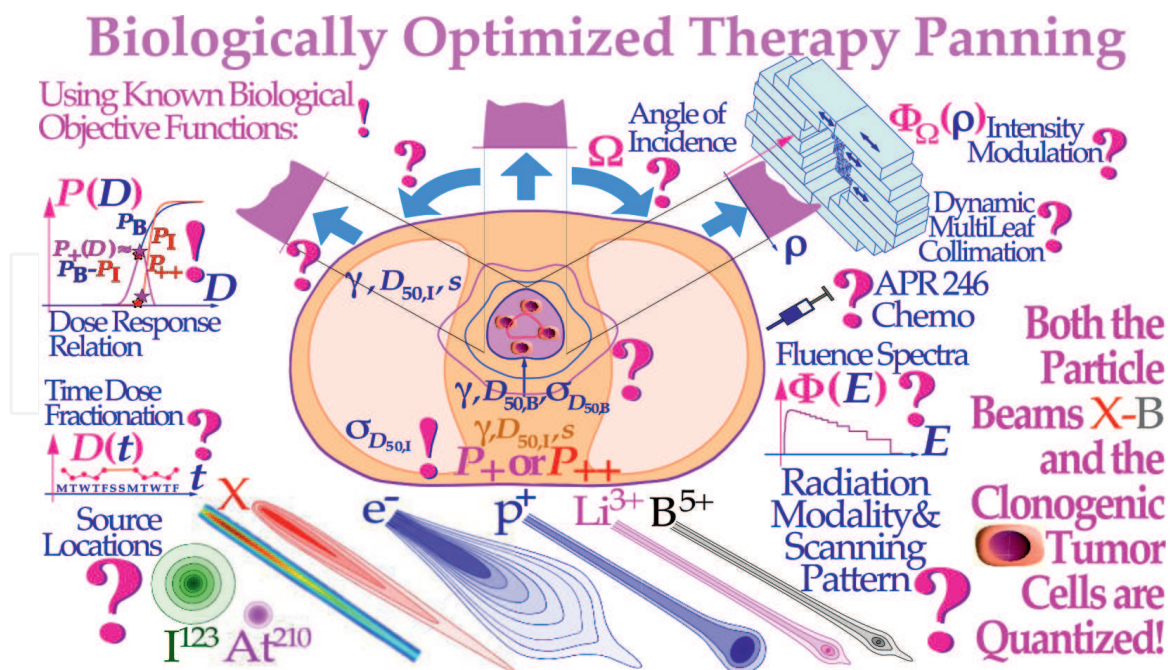


Figure 1.

*Illustration of the fantastic power available by using biologically optimized inverse radiation therapy planning [2]. If we know the approximate sensitivity of the tumor and the normal tissues (!), it is possible to derive the biologically optimal beam directions and their intensity modulation (?; [3]) and it is even possible to find the optimal combination of low and high ionization density radiations (cf. **Figure 15**) and their incident energy spectra as well as the ideal time dose fractionation [1, 4, 5] using biological complication free cure ($P+$) optimization strategies ($P++$: $P+$ with concomitant injury minimization [3]). In addition, if we have information about the interaction of the radiation modality of interest with chemotherapeutic agents of preference, the combined treatment schedule can also be optimized in biological terms. During the last week of treatment, only a hand full of tumor clonogens remain, and should thus preferably be treated with more microscopically uniform electron or photon beams. This is optimal since both the particle beam and the tumor cells are quantized and may protect some tumor clonogens from lethal hits by inevitable cold spots between the ions during the last most curative therapeutic dose fraction [1–5]!*

effect on radiation-resistant tumor cells is as high as possible from a radiation biological point of view [2]. With the lightest ions above protons: He, Li, B, and C the border region between the clinical gross tumor and target volume and surrounding healthy normal tissues can be set as narrow as physically possible. In addition, the optimal number of treatment fractions can be substantially reduced, and the curative gain factor on radiation resistant hypoxic tumor cells may generally be more than doubled compared to low ionization density photons, electrons, and protons. **Figure 1** shows how the optimal selection of Therapeutic beams can be arranged and the energy modulation shaped to maximize the cure probability of the patient with minimal risk for side effects in normal tissues [2]. Largely based on clinically established dose-response parameters of normal tissues (γ, D_{50}, s).

2. Radiation biology of radiation therapy

2.1 Handling of DNA damage by the TP53 gene

The new interaction cross-section based Repairable-Homologous-Repairable damage formula for radiation-induced cellular inactivation, repair, misrepair, and apoptosis in TP53 intact and mutant cell lines can be used to optimize radiation therapy. The formulation requires renewed thinking about the biological

optimization of radiation therapy. It suggests that most TP53 intact normal tissues are Low Dose Hyper Sensitive (LDHS, see left insert of **Figure 2**) and that the inherent microscopic heterogeneity of higher Linear Energy Transfer (*LET*) ion treatments the last week would benefit from low *LET* as shown in the lower right of **Figure 2** [1, 4, 5]. The ability of the new method to quantify apoptosis [1], has helped identify the early Low Dose Hypersensitivity (LDHS) and Low Dose Apoptosis (LDA) of most normal tissues and tumors with intact TP53 and ATM genes. This mechanism has probably been developed by nature's pros of survival advantage selection, to ensure minimal risk for severe mutations to the genome before the DNA repair system is fully functional after around a dose of 1Gy [1, 4–8]. As a compensating measure the apoptosis-inducing caspase 3 gene product (**Figure 2** right) remarkably “remembers” this low dose apoptotic cell loss and starts cellular repopulation to reestablish homeostasis in the tissues after being irradiated.

This useful mechanism in normal tissue is a well-known problem after suboptimal radiation therapy where it can cause accelerated repopulation of remaining tumor cells at the end of treatment [9]. A clear curative intent is probably the principal way to avoid this tumor-reactivating mechanism. These studies also identified that maximum apoptosis is induced by the lowest *LET* ions largely as they have the highest fluence of δ -electron apoptosis induced by primary ions per unit dose [1, 4]. With a too high *LET* the apoptosis and senescence will instead be high in the normal tissues in front of and behind the tumor, which may be undesirable from a complication-free

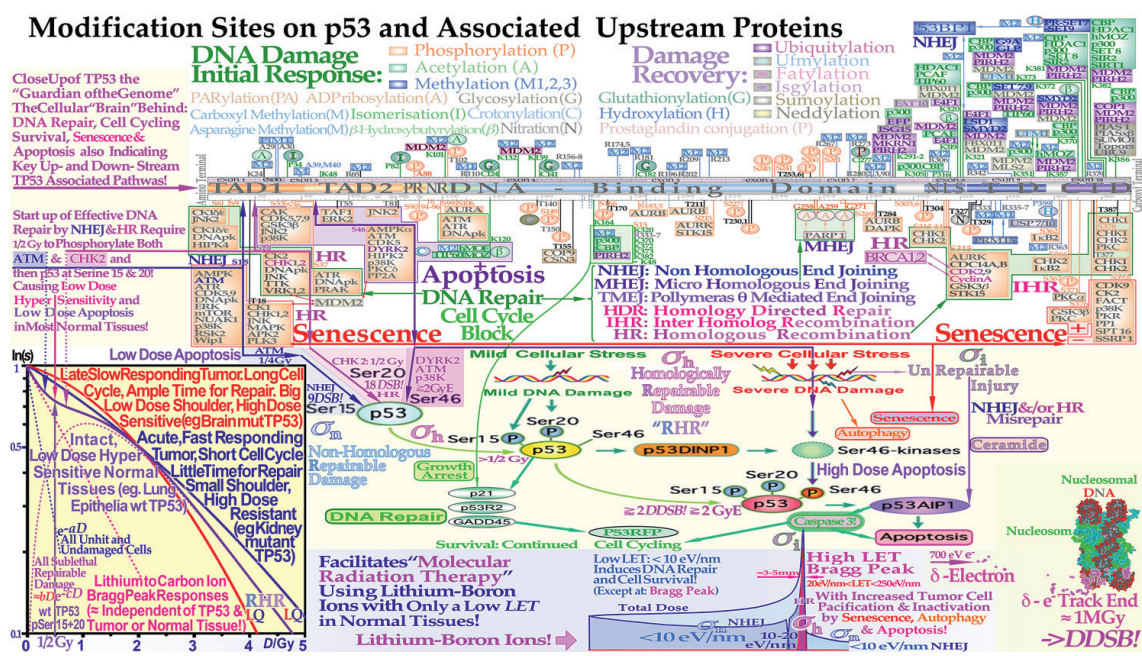


Figure 2. The complex responses of the TP53 gene to mild and severe genetic stress is largely determining the cellular response to radiation [1–13]. Mild stress phosphorylates the serine 15 and 20 sites on p53 by ATM and CHK2, resulting in cell cycle block and DNA repair. This results in LDHS in normal tissues but generally not in tumors often with a mutant TP53 gene as seen in the cell survival insert. Local high doses or high ionization densities resulting in DDSBs (Dual Double Strand Breaks cf. **Figure 3**) [2, 14] are increasing the severity of the damage phosphorylating also the serine 46 site e.g., via DYRK2, p38K, or ATM, and a high dose apoptotic (HDA) response may get triggered. Lithium-Boron (cf **Figure 12**) ions allow unique therapeutic use by inducing a massive apoptotic-senescent tumor cell response within the Bragg peak (σ_n homologically repairable damage and σ_d direct inactivation cross-sections cf. **Figure 4** [1, 4]), but in front of and beyond the Bragg peak, the LET is low, and non-homological easily repairable damage is mainly induced (σ_n cross-section see **Figure 4** insert [1: Figure 8, 4, 7, 8]).

cure point of view, even if hypoxic tumors may marginally benefit from a high *LET* (cf [4] and **Figure 3**).

2.2 Dual double strand breaks

The severe Bragg peak damage to supercoiled DNA first wound two times around nucleosomes in the cell nucleus is shown in the lower right corner of **Figure 2** and the close-up in **Figure 3**. Most toxic are the ≈ 700 eV electrons that deposit a dose in the neighborhood of the track of up to 10^6 Gy as seen in the right of **Figure 2** [1, 4, 14, 15]. In front of the Bragg peak, the density of electrons is lower and even more so in the high energy entrance region requiring many more ions to deliver a dose of around 2Gy (cf **Figure 7**). This phenomenon explains why the medium and low *LET* ion beams are most efficient in inducing apoptosis (as further seen in **Figures 11** and **13**) and thereby eradicating hypoxic tumor cells. With a low *LET*, too few severe direct cell kill events are obtained and at high *LET* too few ions are available at a given dose even though they produce very severe damage. The most probable DNA fragment length at high doses is around 78 base pairs, corresponding to a single turn around the nucleosome (cf **Figure 3**). A δ -electron track end that may randomly hit the DNA at any point on the periphery of the nucleosome and then often produce a Dual DSB (DDSB), can easily produce such fragments. This will very often make DNA fragments of close to a single nucleosomal DNA turn in length as seen in **Figure 3**. This string of DNA may easily be lost as a micronuclei or get inserted erroneously to make a severe mutation and possibly a non-functional protein. Fortunately, most simple DSBs are repaired

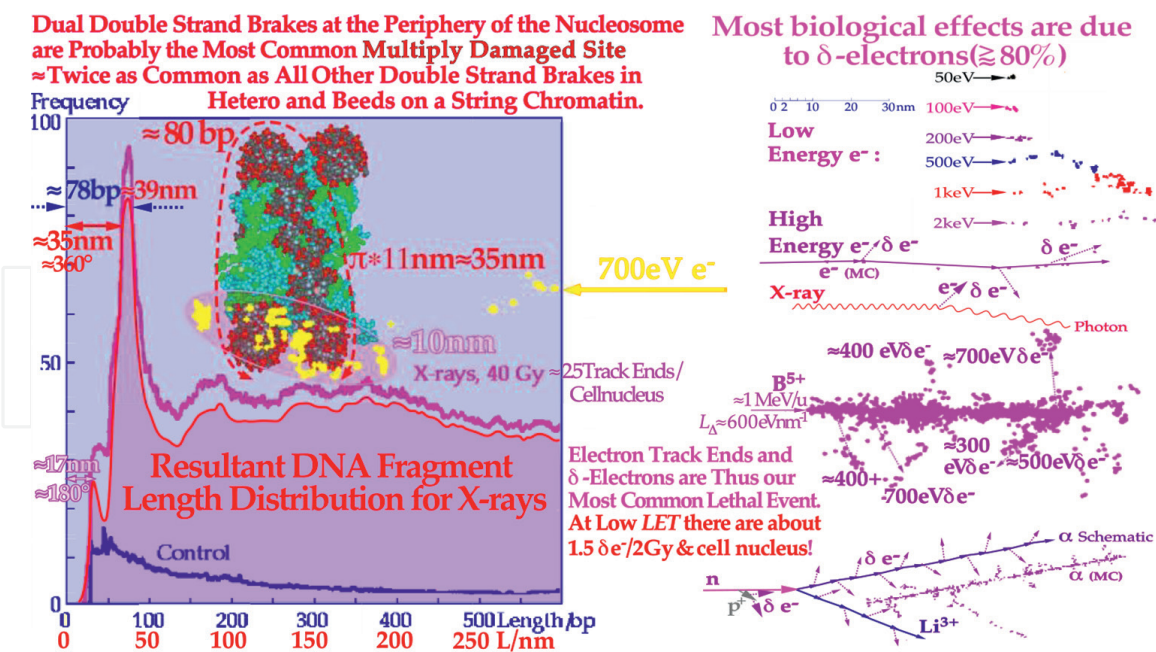


Figure 3. Molecular close-up of ion tracks (right) showing that most of the lethal cell damage of densely ionizing ions is induced by low energy δ -electrons in the 200 eV to 1 keV energy range generating severe difficult-to-repair DNA damage in the cell nucleus such as dual DSBs at the periphery of the nucleosome (left, cf. [14]). The left insert shows that the most common DNA segment length corresponds to a single turn of DNA around a nucleosome as expected from the DDSBs at the periphery of a nucleosome. Interestingly, the 78–80 base pair fragments are about twice as common as all other fragment sizes and they should be expected to be even more common with high *LET* beams having ≈ 3 times more secondary δ -electrons in the sub-keV energy range, with a very high probability of inducing lethal DDSBs.

correctly (>99%) so a DDSB is really the most common multiply damaged site causing severe cell loss [1, 4, 14, 16].

2.3 Cell survival

In two recent DNA repair-based publications [1, 4], the accurate quantification of the cellular survival and damage to tumors and normal tissues are developed to significantly improve our ability to precisely describe the survival to low and high ionization density (*LET*) radiations and doses $S = e^{-aD} + bDe^{-cD}$, far beyond the possibilities of the conventional linear quadratic cell survival model ($S \approx e^{-\alpha D - \beta D^2}$).

Not only are the undamaged cells (e^{-aD}) separated from the sublethal damaged cells (bD) but also the two major DNA damage repair pathways, namely homologous and non-homologous end joining DNA repair (HR, NHEJ) can each be identified ($b_h De^{-chD} + b_n De^{-cnD} \approx bDe^{-cD}$) and so can their complex interactions cf.

Figures 4 and **5** [1].

It is therefore given the name the repairable-homologous-repairable or RHR-formulation as seen in the left insert in **Figures 2** and **4** (cf [1, 4] for further details). The fractionation window linked to LDHS normal tissues as seen in the left insert in **Figure 2** indicates that the low *LET* dose to organs at risk should be ≈ 2 Gy/Fr as this produces the least damage per unit dose, whereas the tumor dose should be substantially higher to ensure perfect tumor cure [5]. This calls for biologically optimized treatments using a few intensity-modulated beams [3] to avoid secondary cancer risk and get a true curative intent, avoiding caspase 3 induced accelerated tumor cell repopulation (see right part of the middle half of **Figure 2**, [9]). Light ions with the lowest possible *LET* in normal tissues and high *LET* only in the tumor indicate lithium to boron ions [5]. The high microscopic heterogeneity in the tumor will cause local microscopic cold spots. Therefore, the last week of curative ion therapy, with few remaining viable tumor clonogens randomly spread in the target volume, as indicated in **Figure 1**, should receive the last 10 GyEquivalent by low *LET* ensuring perfect microscopic tumor coverage and high cure and reduced risk for adverse reactions in normal tissues [5]. Interestingly, such an approach would also ensure a steeper rise of tumor cure and a higher complication-free cure as few remaining clonogens are fairly well oxygenated eliminating shallower tumor response by ion heterogeneity (see **Figure 17**). Avoiding ion microscopic heterogeneity in normal tissues increases complication-free cure both at the low dose normal tissue complication side and high dose tumor cure end of the treatment [5].

2.4 Apoptosis induction

The major forms of interaction between homologous and non-homologous DNA repair such as homologous repair of non-homologous misrepair are accounted for and the probability to induce programmed cell death (Apoptosis) and potentially even more so, permanent cell cycle arrest (Senescence) as well as other cell cycle losses [3, 4]. Interestingly, these processes are probably the optimal ways to inactivate a tumor with minimal inflammatory response and without massive immediate tumor decomposition. Interestingly, lithium ions and its neighbors helium, beryllium, and boron ions have an important and unique potential to induce apoptosis locally, mainly in a few mm-size volumes around their deep high ionization density Bragg peaks in the tumor as seen in **Figures 4**, **5** and **7** (Be may be associated

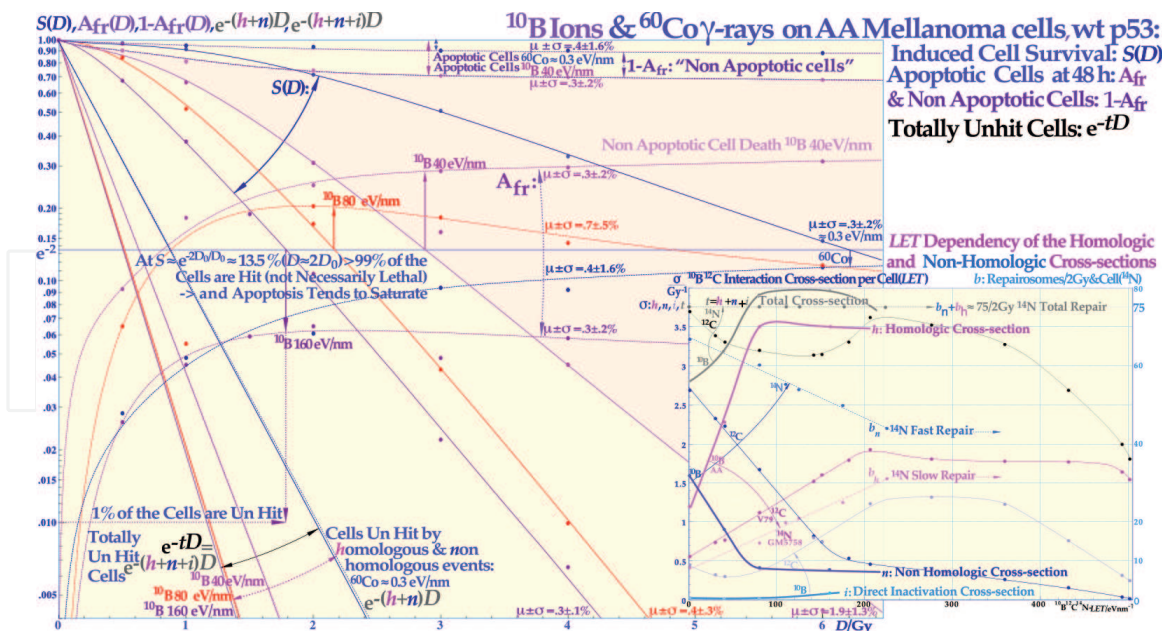


Figure 4. The cell survival, the cell fractions that are totally un-hit by the beams, and the apoptotic and non-apoptotic death over the LET range 0.3-40-80-160 eV/nm from ^{60}Co and boron ions. The cell survival shows a gradual increase in steepness with increasing LET whereas the A_{fr} has its maximum at a dose causing around 13.5% cell survival as indicated by the arrows. For the two lowest LET's, the non-apoptotic cells, upper dashed curves, and the clonogenic survival are practically tangential at low doses indicating apoptosis is the preferred way of cell death before p53 is phosphorylated at its Serine 15 and 20 sites at $\approx 1/2$ Gy (Figure 2). The shaded area is due to non-apoptotic cell death for 40 eV/nm boron ions showing the domination of apoptotic cell death at the low LET's as the shading is lost at low doses. The survival data are also used in Figure 14 on a linear scale to derive the secondary cancer induction probability. The associated LET variation of the non-homological and homological interaction cross-sections n and h for DNA repair after ^{10}B irradiation but also for ^{12}C ions, as shown by the insert [1, 4]. A comparison with the variation of the fast b_n and slow b_h repair of repair some foci after ^{14}N irradiation (dashed lines, right scale, data derived from [4, 17]). The homological cross-section h increases very fast with the LET for ^{10}B ions due to rapidly narrowing δ -electron cores and so is the associated reduction of the n cross-sections.

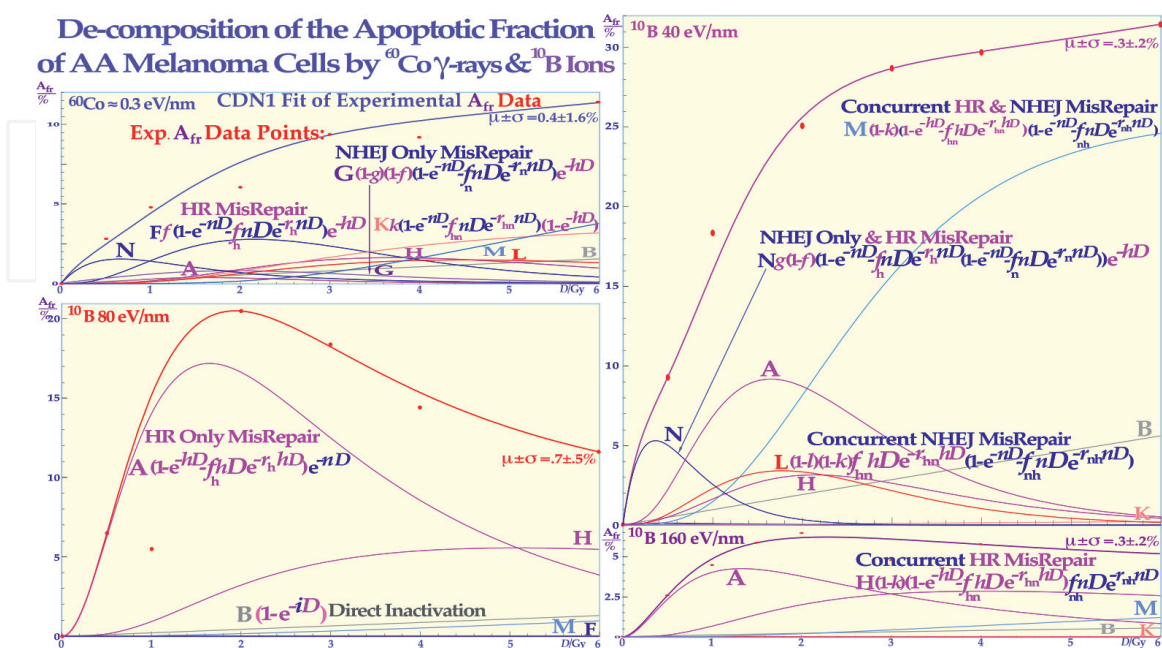


Figure 5. The LET variation of the apoptotic fraction contributions of the eight key misrepair processes A-N indicating a relative apoptotic effectiveness (RAE) of about 3.4 for low LET boron ions around 40 eV/nm, whereas the peak relative biologic effectiveness (RBE) is about 3.5 but closer to an LET of about 140 eV/nm (Modified from [1]).

with additional BeO forming toxicity in the tumor but also in normal tissues (cf. **Figures 11** and **13**). Everywhere else they mainly induce low-ionization density and LET-type effective DNA repair processes as seen in the right part of **Figure 2**. The surprisingly popular proton therapy has an almost negligible such augmented local high biological tumor effect, helium has some, lithium, beryllium, and boron have more and more, and finally the already rather promising carbon ions have a little too much, both in the entrance region with mainly normal tissues and the fragmentation tail beyond the tumor, and not least up to as far as 5 cm in front of the Bragg peak (cf **Figure 12**). Boron ions are therefore most likely the optimal ion for medium to large tumors whereas for small to medium size tumors and not least pediatric tumors a combination with lithium ions may be the most optimal for clinical use (cf **Figures 2** and **15**)! Interestingly, the lightest existing positron emitter Boron 8, makes it possible to immediately visualize the delivered dose to the patient by Positron Emission Tomography (PET) and verify that optimal dose delivery is achieved in the tumor region.

2.5 Relative biological effectiveness

With increasing atomic number, the penumbra gets narrower and the longitudinal range straggling is also lower, so more of the energy is deposited in the tumor by light ions of increasing atomic weight and Relative Biological Effectiveness (*RBE*) as seen in **Figure 6**. The high energy deposition density at the end of the ion range (the Bragg peak) is caused by a velocity resonance increasing the energy transfer to the tumor cells when the speed of the ion is close to the speeds of the orbital electrons of the tumor tissue and there is an increased probability for high energy transferred from the multiply charged ions to the electrons as they travel longer distances together toward the end of the particle range. The resulting peak is seen in **Figures 2, 6–8, 11** and **12**. When the atomic weight gets too high, the amount of particle fragments increases, so the dose beyond the Bragg peak gets high too, as seen in **Figures 12** and **13**. Ions heavier than carbon should therefore be used very carefully with sensitive normal tissues in front of and beyond the tumor.

3. Physical, biological, and clinical properties of light ion beams

Compared to low *LET* photon, electron, and proton beams, the clinical properties of light ion beams for radiation therapy are much more versatile and complex as discussed in more detail below. A large part of the detailed specific information is presented in graphical form in the Figures and their captions for simplicity and clarity.

3.1 Ion pencil beams

The physical and biological properties of narrow beams of the six lightest ions when penetrating water to a depth of 30 cm by their central axis energy deposition density profiles already shown in the lower row of **Figure 1** in 2D are described in 3D. The influence of multiple Coulomb scattering and longitudinal range straggling on the Bragg peak of the pencil beams is clearly shown in **Figure 7** (see also **Figures 8–10** below). With protons, the dose to normal tissues in front of the tumor is twice the

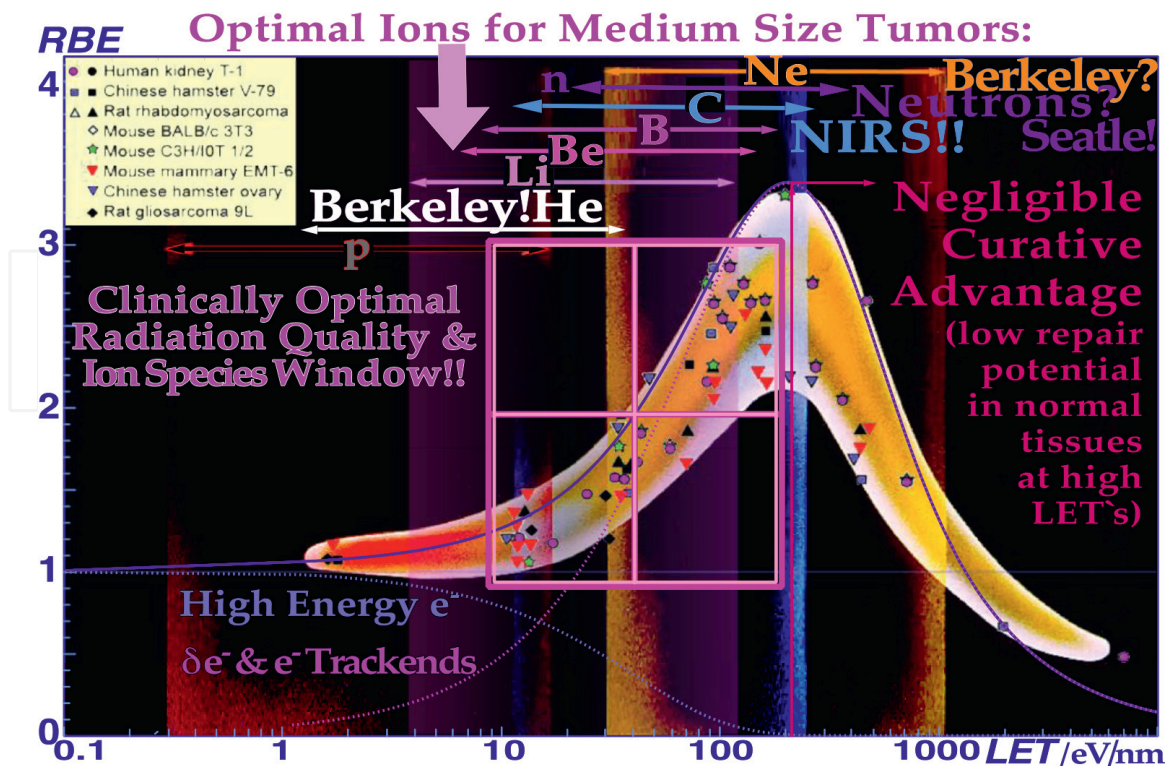


Figure 6.

Comparison of the RBE and LET ranges available with protons, lithium, boron, carbon, and neon ions is shown. It is seen that the range from lithium to carbon ions is most interesting, especially for hypoxic tumors. In general, LETs beyond the RBE peak should be avoided to minimize normal tissue damage in the entrance and plateau region (C-Ne, cf. **Figure 2**). As the cross-section saturates (cf insert in **Figure 3**), the relative biological effectiveness RBE reaches a maximum since the cross-section cannot increase with the LET anymore, and at higher LETs the biological effectiveness decreases because of an increased probability of radical-radical recombination as secondary electrons are generated more and more closely together. Furthermore, the “overkill” effect implies that multiple kill events are equal to a single kill (you can only die once). The dashed and solid curves [18] describe the average response of the multiple experimental data sets very well [19].

tumor dose due to significant multiple scatter whereas it is only a small fraction of the tumor dose for the light ions of lithium, boron, and carbon. This makes the local increase in dose to a small region of normal tissues in front of the tumor about five times larger than the increase in tumor dose that may be needed for tumor cure. This demonstrating that for each dose addition to a small part of a tumor volume will require that about five times more doses have to be given to normal tissues in front of the tumor with protons as compared to other light ions from lithium to boron. This is a severe dose delivery disadvantage for small radiation-resistant tumors and extra beam portals may be needed to avoid normal tissue damage with protons. It may be less of a dosimetric problem for large tumors where the broad beam Bragg peak dose level is better established. However, large tumors often have extensive hypoxic regions so protons are not generally the radiation modality of choice, and lithium to boron and even carbon ions are more often indicated for larger hypoxic tumors. The shapes of the so-called narrow pencil beams in **Figure 7**, therefore, are a kind of figure of merit when using inverse biologically optimized treatment planning trying to maximize the patient fraction that is cured without severe damage to normal tissues [3]. A high distal the so-called Bragg peak is therefore important and so is a low dose in the entrance and exit regions to minimize normal tissue damage in front of and not least behind the tumor by nuclear fragmentation as seen in even more detail for Boron and Carbon in **Figure 12**.

Ion Pencil Beam Energy & Dose Deposition Kernels

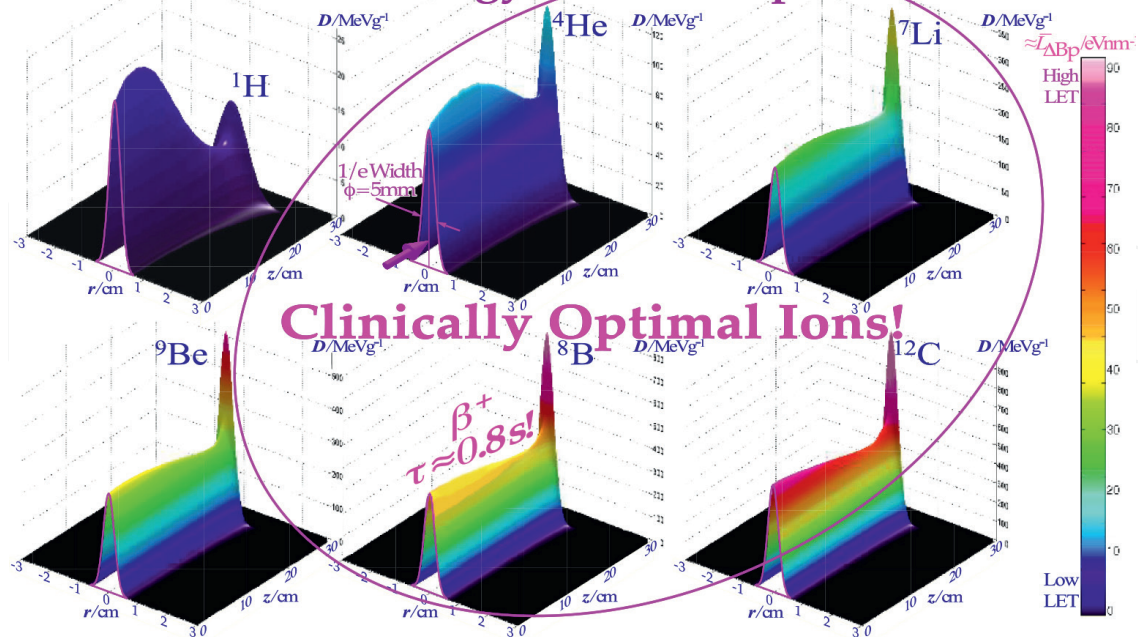


Figure 7.
 3D Illustration of the clinical value of different 5 mm 1/e width light ion pencil beams for biologically optimized therapy planning. For carbon ions and heavier, the increasing LET in the plateau-type entrance region has to be considered more carefully when maximizing the probability of reaching a complication-free cure. The color scale illustrates the ionization density (LET) and consequently the increased biological effect in the tumor, which comes as a very important biological advantage on top of the physical dose distributional advantage shown in the figure.

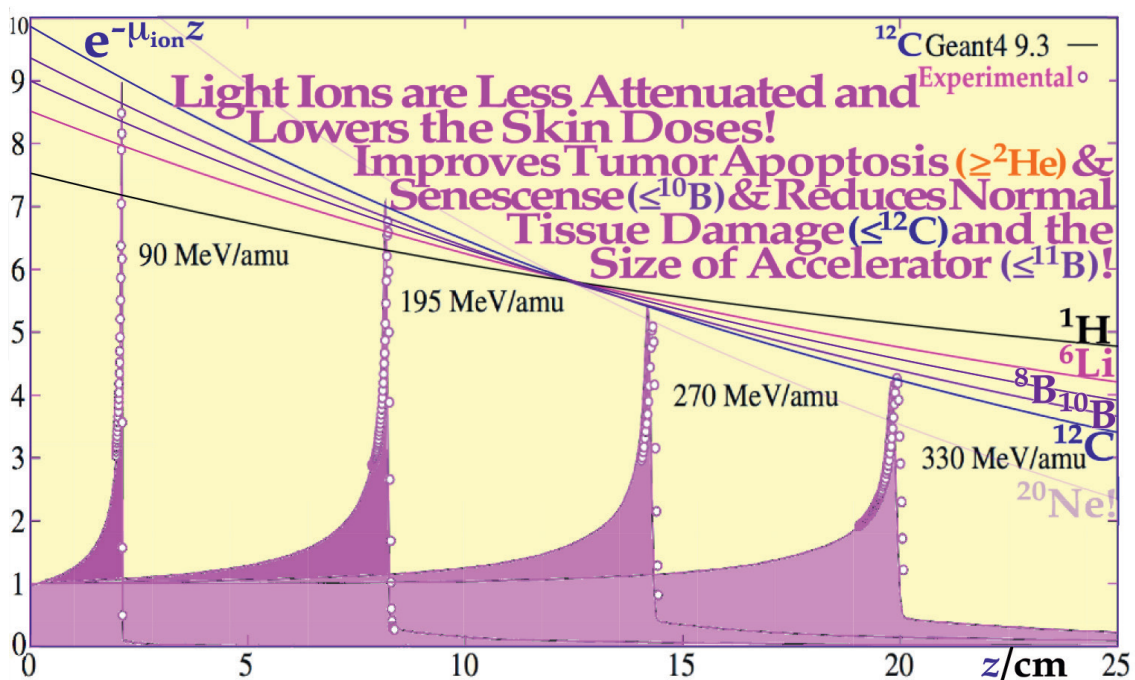


Figure 8.
 As the cross-section increases with nuclear size light ion attenuation will be less in the normal tissues of the patient, to more effectively reach a deep sited tumor! Hydrogen would thus be optimal from this point of view but the biological effect is minimal as seen in Figures 2 and 4, making He, Li, and B more interesting!

3.2 Exponential ion attenuation

Like Photons, Light ions are attenuated exponentially but by nuclear reactions rather than by photoelectric, Compton, pair, and photonuclear reactions. Protons are only weakly attenuated, less than 50 MV photons, whereas carbon ions are similarly attenuated as 16 MV photons and neon more like 4MV and almost ^{60}Co . Part of the clinical problem with Neon ions is very clear as they are severely attenuated at large depths. **Figure 6** shows the other part of their problem as their entrance regions have a very high RBE and they reach far into the overkill region at depth as also seen in **Figure 11**. The merits of the light ions from lithium to boron are clearly shown in the figure all with an attenuation less than that of a 45 MV Betatron beam. Furthermore, to reach 25 cm of tumor depth a 400 MeV/u carbon ion beam may be needed whereas 300 MeV/u boron may suffice, thus requiring a smaller and less costly cyclotron for beam production as seen in the figure.

3.3 Particle multiple coulomb scattering

The increase in the penumbra (distance between 80 and 20% isodose lines) as a function of depth in water is shown in **Figures 9** and **10**. The Multiple Coulomb Scattering in the patient will increase the penumbra substantially with depth since the scattering power increase with decreasing energy. On top of these, multiple scatter contributions ($r_{1/e} = \sigma_r$) the part from the initial effective source size (σ_0) of the intrinsic accelerator beam should be added in quadrature as they stem from statistically independent processes so the total standard deviation is given

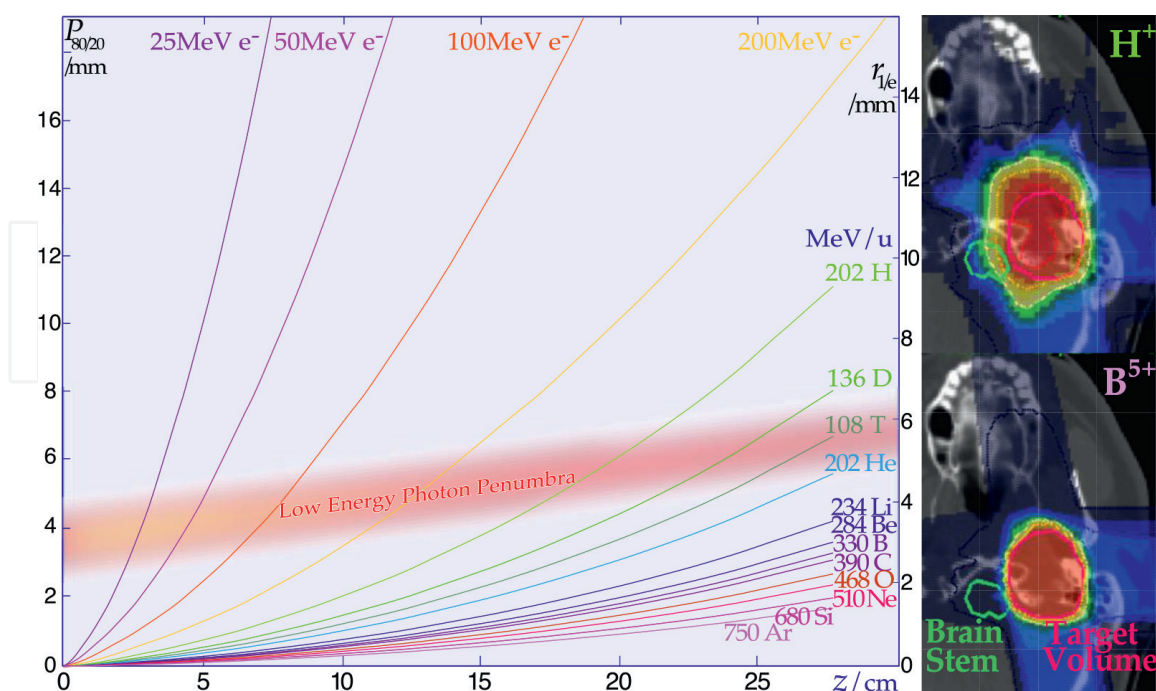


Figure 9.

With electrons and protons, the penumbra width is better than for photons at shallow depths (<5 cm), whereas light ions from helium and beyond are needed to get significant improvements compared to photons at large tumor depths. The insert shows the clinical advantage of a sharp penumbra in the neighborhood of organs at risk. The brainstem in this case is almost totally avoided with carbon or boron ions but not with protons (courtesy Jürgen Debus, Heidelberg).

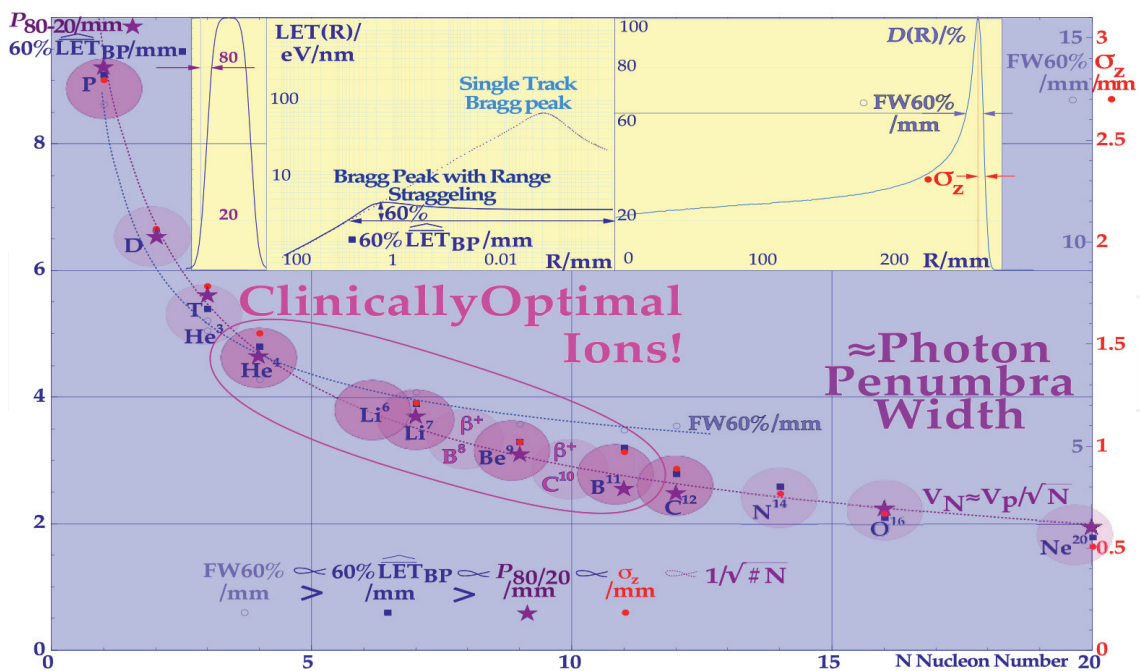


Figure 10. The variation of the lateral penumbra and longitudinal Bragg peak width and range straggling for light ions of increasing nucleon number. A sharp reduction to 50% of the wide half-value width of protons is seen for helium and about one-third for lithium and about a quarter for boron and beyond.

by $\sigma_{\text{tot}}^2 = \sigma_r^2 + \sigma_0^2$. This initial part is included in **Figure 7**, where $\sigma_0 = 2,5 \text{ mm}$ (1/e width = 5 mm). The clear improvement in tumor coverage and normal tissue avoidance is seen in **Figures 9** and **10**, where also the reduction in penumbra width is seen beyond helium ions. In **Figure 10** the initial very steep reduction in the lateral penumbra and the longitudinal range straggling when going from protons to helium and more gradual going from helium to lithium, boron and carbon is clearly demonstrated. Since the penumbra of helium ions (α -particles) is already half of that for protons, helium ions are really the particle of choice in the low *LET* region as they in addition have very clear biological advantages not least in hypoxic tumors (cf **Figures 2, 6, 7, 9** and **11**).

3.4 Lateral penumbra width and longitudinal range straggling

The lateral multiple scattering and the penumbra decrease in almost the same fashion as the longitudinal straggling measured at the 60% width of the high *LET* region of the Bragg peak and they are closely proportional to the inverse square root of the nucleon number as seen **Figure 10**. The full 60% Bragg peak width is approximately the half width of these former quantities as seen in the right insert [20]. One may ask why there is such a large difference in biological effect between protons and other light ions (see **Figure 7**) even though their normalized broad beam dose distributions are fairly similar (cf **Figures 8** and **11**). This is mainly due to the same phenomenon that reduces their penumbra width and longitudinal range straggling with increasing nucleon number as seen in the middle straggling insert in **Figure 10**, reducing the single track *LET* from about 70 eV/nm over some 10 μm to a mean value of about 5 eV/nm in the few mm of range straggling at the Bragg peaks in clinical beams. This also shows up in the small *RBE* variation of protons in **Figure 11**.

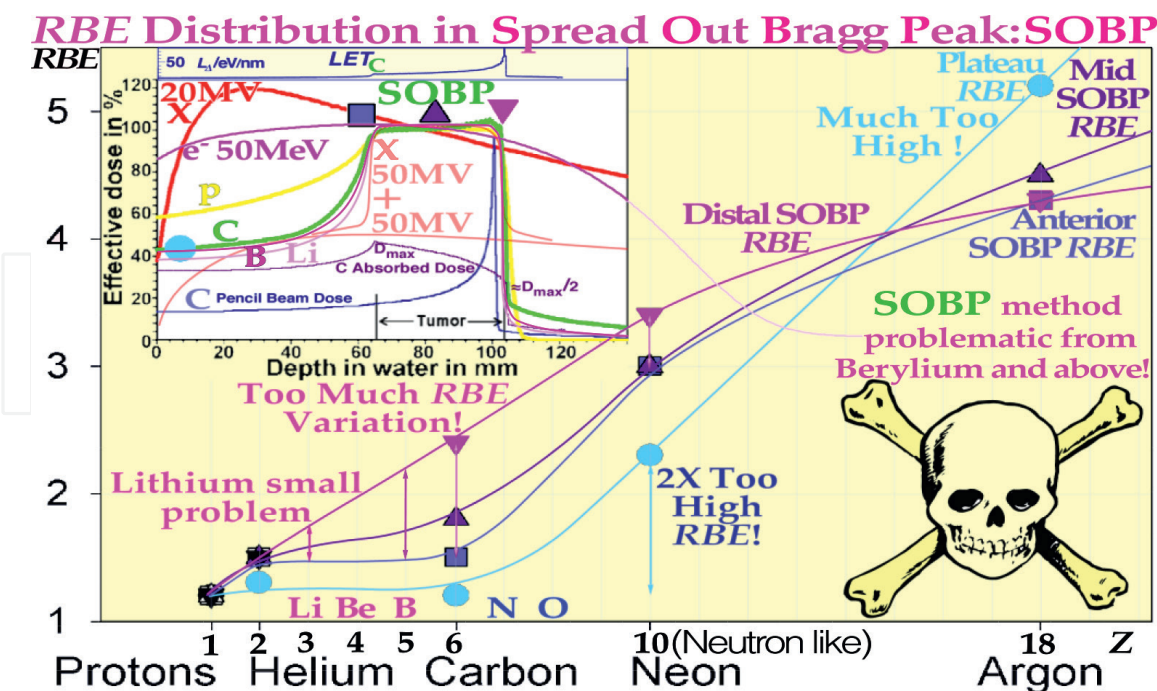


Figure 11. The Variation of the biological effect over the SOBP will make the dose at the distal target volume low and LET high making the risk for microscopic cold spots high and increasing the risk for a recurrent tumor [5]. With high energy electrons and photons two perpendicular beams make a better high-dose dose distribution than a proton SOBP even if the low dose is lower, making Li, B, and C ions most interesting from a therapeutic point of view. With B and C ions, the method with two different intensity-modulated beams will eliminate the single beam SOBP problem as shown in Figure 15.

3.5 The RBE variation in the beam

The traditional way to make a uniform dose in an extended tumor volume is to use the so-called Spread Out Bragg Peak (SOBP) method first developed for protons at Berkeley and Uppsala where the energy and thus the range was modulated to get a uniform dose in the tumor volume [21]. This works well for protons with almost negligible biological effect variation with depth as seen in Figure 11. However, with Boron and Carbon ions there will be a substantial RBE variation with depth so the distal dose will be about half of that at the anterior part of the tumor generating an approximately uniform mean cell kill but a about twofold variation in biological effect as seen in Figure 11. This is far from desirable for a uniform tumor or even a heterogeneous tumor as seen from the large RBE variation measured for carbon ions in Figure 11. Combining lithium and boron ions in suitable ratios is better (Figure 15).

3.6 LET variation in beams

To clearly show the physical and biological differences between boron and carbon ion beams their partial ionization density contributions along with their absorbed dose distributions are shown in Figure 12. Even if their physical dose distributions are quite similar as already seen in Figure 7, their local ionization densities and LET's are rather different with the whole entrance region of carbon being of medium LET. With boron, this region is mainly low LET and the high LET region only extends ≈ 2 cm in front of the Bragg peak whereas it is about 5 cm for carbon ions. Furthermore, there is negligible elevated LET behind the Bragg peak of boron, so normal tissues both in front of and behind the tumor are much less damaged by boron therapy which is an

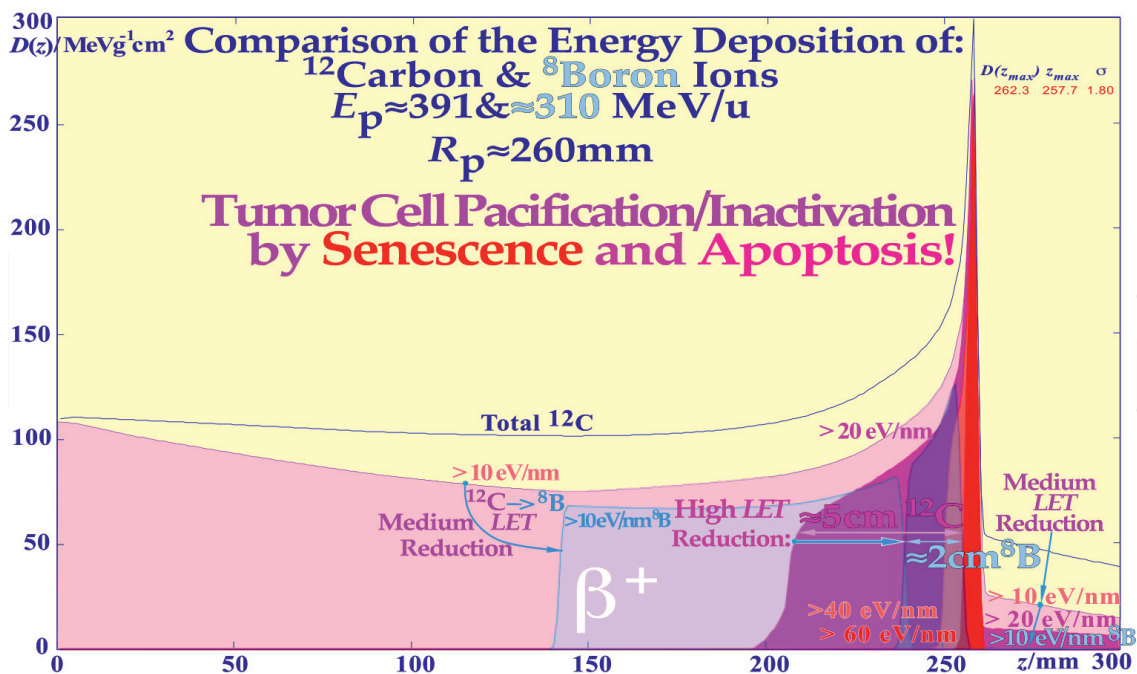


Figure 12. Carbon and boron ion beam depth distribution of the energy deposition density. It is clearly seen that the adverse Biological effect in the entrance and fragmentation tail regions are significantly reduced by boron ions. With sensitive organs at risk in front of and behind the tumor volume, the high LET reduction will also be a further important advantage of boron ions as they will generate more apoptosis in the tumor than carbon ions as seen in Figure 16.

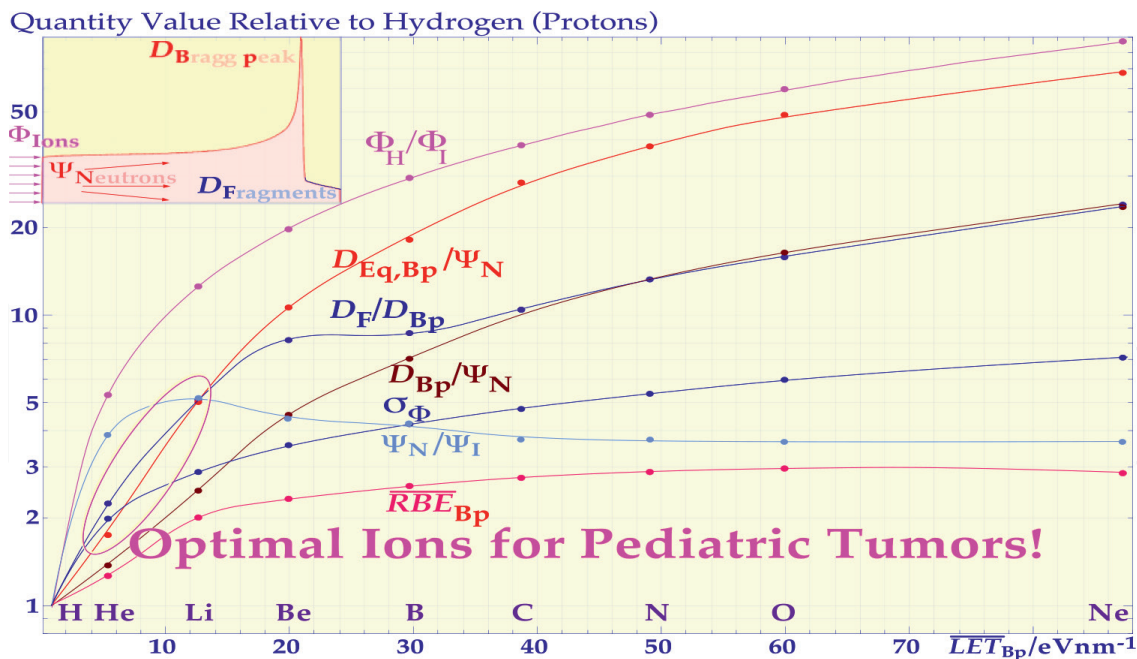


Figure 13. Ion absorbed dose per neutron energy fluence. The increase of the RBE, the Bragg peak and fragmentation tail doses, D_{Bp} and D_{F} per unit neutron energy fluence, Ψ_{N} , and ion fluence, Φ_{I} , at tumor lethal doses of light ions as a function of the mean Bragg peak LET values are shown. All the values are given relative to those for protons and the curves clearly show how much higher the fluence of protons is compared to other light ions up to neon at a given biological effect. Furthermore, the increase in therapeutically effective dose in the Bragg peak per generated unit of neutron energy fluence, the ratios of tail fragment dose compared to the Bragg peak dose, the Bragg peak absorbed dose per neutron energy fluence, the increasing variance of the particle fluence as caused by the reduced fluence of ions at high LETs and RBEs, and the mean ion Bragg peak RBE are all shown in order from top to bottom.

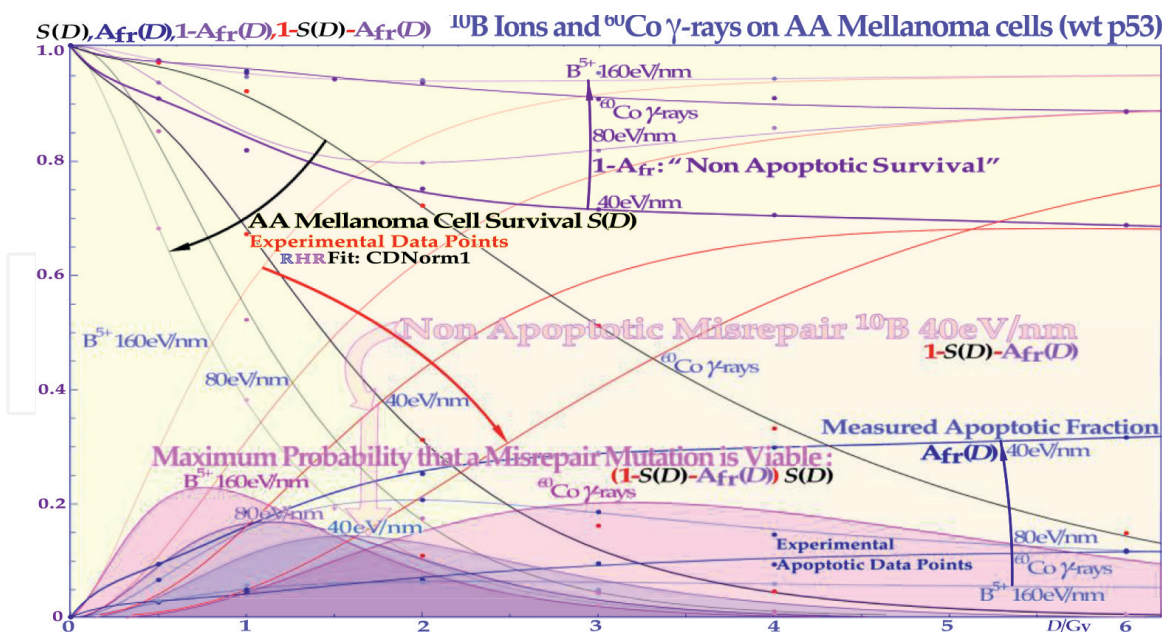


Figure 14. The probability for secondary cancer induction as a function of the dose delivered to normal tissues. At low doses the risk of inducing a mutation is small, at high doses the probability to generate it is higher but so is the probability to eliminate it by the treatment. The risk is high in normal tissues between 0.5 and 6 Gy so this volume in the patient should be minimal! The LDA and LDHS of this TP53 intact cell line are clear! Interestingly, the risk is the smallest for the lowest LET boron ions due to HDA! CDN1: One-dimensional closest distance norm (not least square!). Based on data from [1, 5].

important clinical advantage! This makes boron ions most suitable for mixed beam therapy as is more clearly shown in **Figure 15**.

3.7 Neutron production

Like high-energy photon beams light ion beams are always associated with a significant neutron production as seen in **Figure 13**. Due to nuclear reactions, the cross-section and number of neutrons produced increases with the increasing atomic number of the projectile as the number of fragmentation reactions and consequently, the number of neutrons increases with nuclear size. However, the number of ions needed to eradicate a hypoxic tumor simultaneously decreases rapidly since the *LET* and *RBE* increase with atomic charge and mass as seen in **Figures 6** and **13**. In fact, **Figure 13** shows that the fluence reduction increases both the dose and the equivalent dose per unit neutron energy fluence generated and thus steadily decreases the neutron production with increasing atomic number of the ion at tumor lethal doses. Interestingly, at the same degree of cell kill, protons produce the highest neutron energy fluence partly because their mass is close to that of the neutron. From beryllium and above, the fragmentation is rather high so helium and lithium are probably the most ideal ion species for the treatment of pediatric malignancies. From the point of view of neutron and light fragment production, the ideal ion is generally somewhere between lithium and boron as seen in **Figure 13** but avoiding beryllium's high fragmentation and potential toxicity. Interestingly, even if the cross-section per ion to produce neutrons goes up slowly with atomic number, about 5, 15, and 40 times higher fluencies of protons are needed compared to helium, lithium, and carbon ions, making the total neutron production the highest by protons at equally curative doses of light ion therapy. Both the mean absorbed

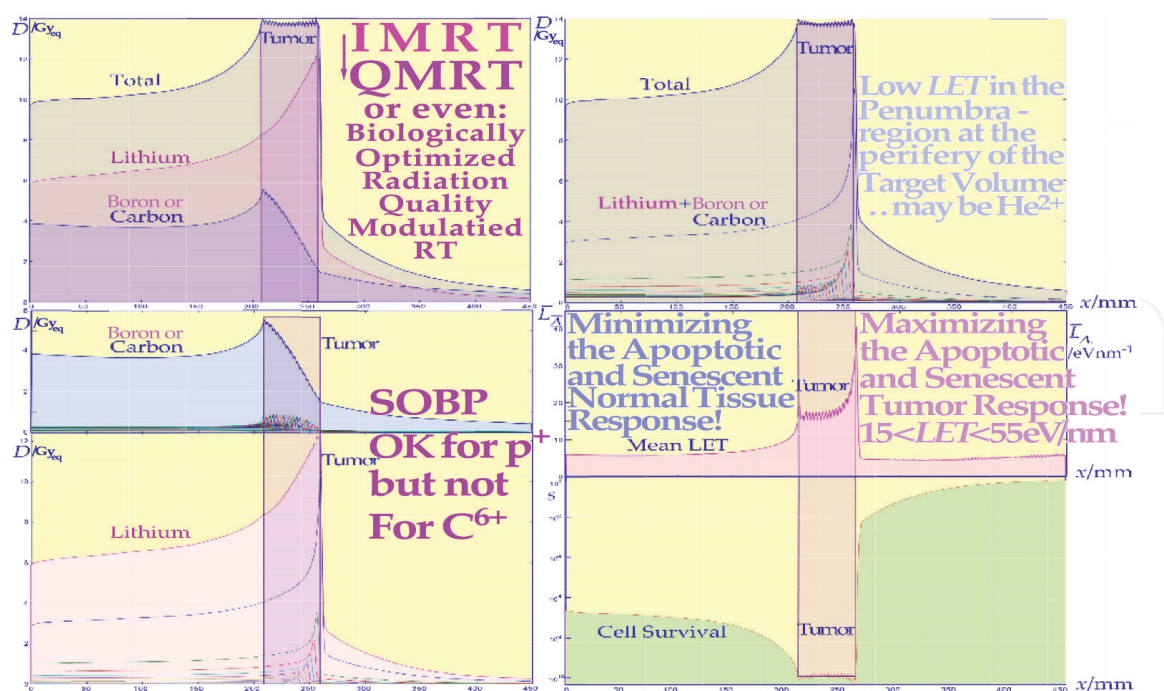


Figure 15. A quasi-uniform absorbed dose and cell kill distribution is generated between about 21 and 26 cm of depth by combining lithium and boron or carbon ions in suitable ratios to make the cell kill and survival quasi-uniform. The small local fluctuations in absorbed dose are due to a somewhat too large longitudinal range modulation (~3 mm) used to clearly illustrate the applied mechanism combining lithium and boron or carbon ion Bragg peaks at each depth interval. The different panels show the total absorbed dose and the boron or carbon doses and the lithium dose in the upper row, whereas the cell survival and mean LET distribution is shown below. Interestingly, by combining lithium and boron or carbon, a uniform biological effect, survival, and absorbed dose can be obtained both for uniform tumors and optimal biological effect modulation for heterogeneous tumors [23].

dose (D_{Bp}) and dose equivalent ($D_{Eq,Bp}$) at the Bragg peak per unit energy fluence of neutrons generated (Ψ_N) increase rapidly with the atomic number as seen in **Figure 13**, indicating that the absolute neutron production reduces steadily with atomic number. The dose of fragments is unfortunately also increasing. Helium and lithium ions are therefore indicated to be most optimal for pediatric tumors where the neutron fluence, dose and biological effect on normal tissues surrounding the tumor should really be minimized to reduce as far as possible the neutron-generated risk for secondary cancers.

3.8 Secondary cancer induction

To further illustrate the power of quantifying apoptosis, **Figure 14** estimates the probability of inducing secondary cancer based on experimental cell survival and apoptosis data [1: Figures 7+9]. It is unlikely that the Apoptotic fraction will contribute to secondary cancer induction (except possibly in TP53 mutant cell lines) so it is useful that this fraction can be estimated by the new RHR formula and be removed from other forms of misrepair to more accurately describe the cells that are potentially capable of generating secondary cancers. This cell fraction, as seen in **Figure 4**, has its peak in the 1-3 Gy range so in radiation therapy optimization, it is desirable to minimize this volume as much as possible in normal tissues. **Figure 14** shows the maximal risk is smallest for low LET ions (blue shaded), the real risk may be in the order of 5% of the values in the Figure. This effect is a contraindication for very many beam portals in intensity modulated radiation therapy e.g., using “rapidarc”, “volumetric

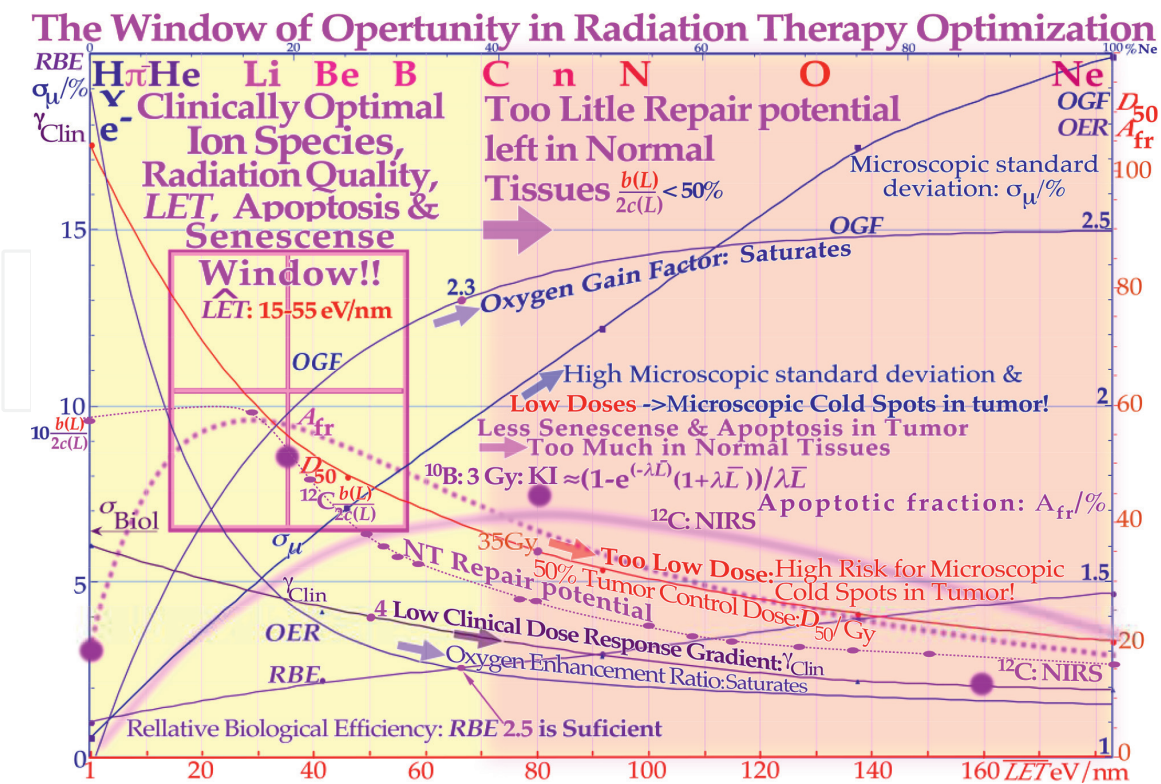


Figure 16. The LET variation of key biological parameters that influence the clinical value of radiation beams showing that the optimal window of opportunity in radiation therapy optimization is located between about 15 and 55 eV/nm or He-B ions. The underlying data are collected from Berkeley, NIRS, and Karolinska.

arc”, and “tomotherapy” like methods on non-seniors, that may have time to develop secondary cancer after some 20 years cf [22].

4. Treatment optimization

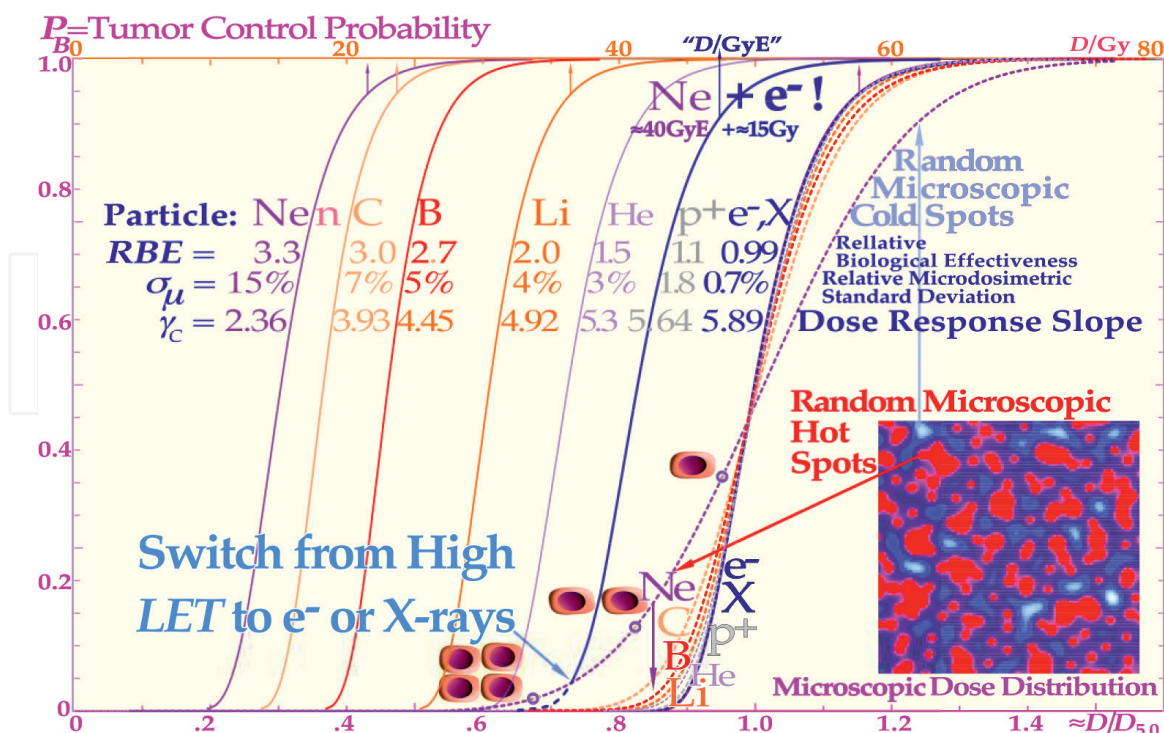
4.1 Generation of uniform absorbed dose and cell kill

It is better from a microdosimetric point of view to generate a rather uniform microscopic energy deposition density on the cellular scale in the tumor to avoid dosimetric cold spots in tumor clonogens [5] that could repopulate the tumor and start with a slightly lower LET at the anterior tumor edge as shown in **Figure 15**. This could in principle be done in two different ways, either starting with a suitable Bragg peak at the distal tumor edge and gradually increasing the atomic weight and Bragg peak LET of the ion used or by just mixing two different ions species so that the mean LET and dose stays approximately constant as shown in **Figure 15**. Interestingly, this latter approach requires that most of the Bragg peak dose in the anterior part of the tumor is of very high LET, such as boron or carbon ions, whereas the distal part mainly requires a lower LET such as helium or lithium ions. In fact, mixing lithium and boron or carbon ions may be the optimal way to achieve close to ideal microscopic energy deposition density distribution for medium-to-large size tumors whereas several small oligo-metastasis are best treated by lithium ions alone. The survival was calculated for simultaneous irradiation whereas the mean LET is based both on lithium and boron or carbon ion components, but the LET variation was low, and

it peaks just downstream from the distal part of the tumor where the dose is a little low. The figure also illustrates the principle of Quality Modulated Radiation Therapy (QMRT) where the absorbed dose and biological effect and radiation quality can be optimally modulated instead of just the Intensity (IMRT) e.g., over a severely hypoxic tumor [23, 24].

4.2 Selection of optimal particle and LET

Based on the cell survival curves in **Figure 4** and apoptosis curves in **Figure 5**, one may ask which ion and LET should be used to maximize the complication-free cure of the radiation treatment. The very flexible method of mixing two ions with largely different ionization densities as shown in **Figure 15**, such as He or Li and B or C, rather than using Spread-Out Bragg Peaks [21], which work well only for protons as seen in **Figure 11**. The SOB method generates strong variations in ionization density and absorbed dose. The variation is a factor of approximately two over the whole target volume for carbon ions, with a too low LET at the anterior end and too low dose and too high LET at the distal part of the target volume as seen in **Figure 11**. This significantly increases the risk of microscopic cold spots at the distal part of the target volume [5]. The use of mixed-modality treatments can make the absorbed dose and biological effect almost constant (cf **Figure 15**), or even locally elevated, e.g., in regions of strong hypoxia [2, 23, 24]. The beam quality question will therefore be discussed in terms of the optimal particle species and mean LET, as shown in **Figure 16** for the LET range from 0.2 to 180 eV/nm covering X-rays-Ne ions as recently discussed [4]. “In this region the RBE increases steadily from 1 to approximately 4.5, the oxygen enhancement ratio (OER) decreases from approximately 3 to almost 1, the normal tissue repair potential $b/2c$ decreases from about 1 to $1/4$, the normalized clinical dose response gradient, γ_C , decreases from approximately 6 to 2 (cf **Figure 17**), the microscopic standard deviation in dose σ_μ increases from 1% to approximately 20%, the 50% tumor control dose, D_{50} decreases from almost 100 to 20 Gy for radiation-resistant tumors, the apoptotic fraction, A_{fr} varies from almost 60 down to $\approx 3\%$ and the oxygen gain factor (OGF) increases from 0 to 2.5. Importantly, above approximately 55 eV/nm, many of these factors become less advantageous for clinical use: the loss of sublethal DNA repair in normal tissues (see **Figure 4** with insert), the saturation of the OER and the OGF, and the reduced senescence and apoptosis in the tumor (**Figure 16**)”. The increase in microscopic standard deviation (σ_μ) will decrease the clinical γ_C value and microscopic cold spots may appear as the standard deviation in dose delivery becomes more significant, as the therapeutic dose reaches ≈ 35 Gy and lower [5]. Consequentially, the senescence and apoptosis in the tumor decrease while it increases too much in normal tissues! Therefore, boron ions are more optimal than carbon ions (**Figure 12**), at least for medium-sized tumors, and lithium ions are the optimal particle for pediatric tumors, and their combination is ideal both for dose and radiation therapy biological effect optimization (**Figures 12** and **15**). It is very interesting to see that the apoptotic and senescent cell fractions have their maxima in the tumor at a much lower LET than the RBE, and it reaches approximately 60% at approximately 30 eV/nm for boron ions (dotted curve in **Figure 14**), whereas the RBE has its maximum at around 140 eV/nm. This is mainly due to the larger number of ions needed per unit dose compared to carbon ions (cf. **Figure 13**). Carbon ions reach only approximately 40% at approximately 80 eV/nm and they may produce unnecessarily high senescence, apoptosis, and LET in normal tissues [4] as seen in **Figure 6**. Optimal


Figure 17.

Microdosimetry of tumor control. Description of the reduction in the normalized steepness, γ_c , of the shape of the tumor control curve for uniform cell line for the different microscopic standard deviation of radiation modalities as a function of the absorbed dose (upper scale) and approximately normalized to the 50% tumor control dose (\approx Dose Eq, lower scale, dashed lines) to more clearly see the effect on the γ_c value as the microdosimetric relative standard deviation increases with the LET. Not only do the hot spots often in the form of dual double strand brakes (DDSB, cf. **Figures 2 and 3**) and cold regions get more extreme with increasing LET, but also the RBE is increasing, reducing the total dose about threefold with carbon, neutron, and neon, increasing the relative standard deviation and reducing the γ_c value more than one would like.

cancer cell inactivation requires a treatment modality that preferentially induces senescence probably the most cost-efficient treatment to stop further cell cycling and block tumor growth. Actually, this is probably the mildest but still efficient endpoint to cure cancer [5, 10, 11, 25, 26], as it can make the clonogenic tumor cells lose their uncontrolled cell cycling ability as seen in **Figure 18**. The induction of autophagy (self-digestion) and apoptosis (programmed cell death, see **Figure 2**) may follow more severe DNA damage to minimize the cancer induction with more complex DNA damage and increased risk for severe mutations, e.g., with turned-on oncogenes or lost suppressor genes. Apoptosis and, even more so, senescence is probably the most optimal way to inactivate a tumor with minimal inflammatory response and without massive immediate apoptotic tumor decomposition [5, 25, 26]. Lithium ions, and its neighbors helium and boron, have an important and unique potential to induce apoptosis locally, mainly in a few mm-size volumes around their Bragg peaks in the tumor, and everywhere else, induce low-LET DNA repair facilitating molecular radiation therapy (see **Figure 2**). In repair terms, this means that NHEJ will dominate in the entrance and fragmentation tail of the ion, whereas HR will mainly try to handle the partly irreparable damage at the Bragg peak, which therefore should solely be placed into the tumor volume [1]. Thus, lithium ions are probably the optimal ion, at least for smaller tumors (see **Figures 2 and 11**, [10]) and pediatric patients. The major advantage of lithium ions is the low-ionization density in all normal tissues, largely inducing fast DNA repair while often inducing apoptosis and senescence only in the tumor volume. For the same reasons, medium size

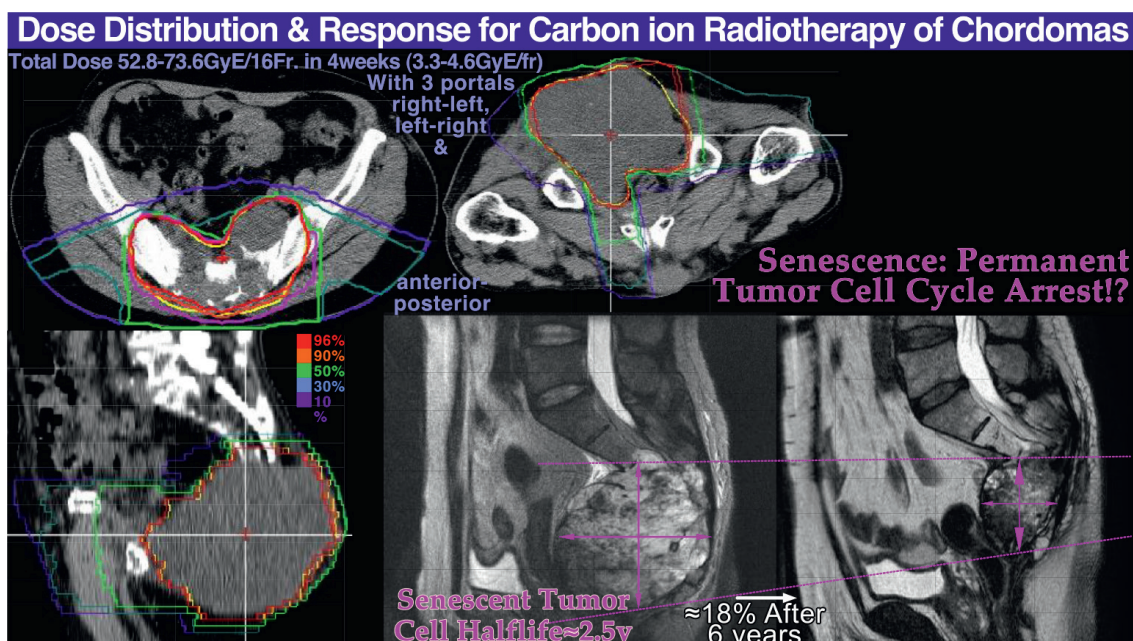


Figure 18. Illustration of the dose delivery for a large pelvic chordoma as shown in the upper and lower left treatment plans. The lower right plain MR images show the gradual disappearance of the chordoma 6 years after the treatment, probably due to a totally senescent response without traces of tumor growth. This treatment was made with carbon ions but could most likely be done with an advantage with boron ions as seen by the B and C ion LET data and apoptosis in **Figures 7–17!** (Courtesy: Hirohiko Tsujii, NIRS, Chiba, Japan).

tumors are probably best treated using boron ions, but this may sometimes require an extra beam portal compared to carbon ions, especially for larger hypoxic tumors. Interestingly, for radiation resistant commonly TP53 mutant tumors (cf **Figure 2** lower left insert) the p₅₃ reactivating compound APR-246 can increase the apoptotic-senescent response and increase the effect of Reactive Oxygen Species [1: Figures 6+17, [5, 25, 27]] and will work well adjuvant also with Boron-ions. Furthermore, ⁸B is our lightest and best direct PET emitter for concomitant online dose delivery imaging, although perhaps a little complex to make [28], and with a very short half-life of ≈0.8 sec so the PET camera really needs to be in the treatment room and used between ion accelerator pulses while treating the patient with the advantage of a rapid malfunction response time (10, 29, Figure 8.37, 8.38f).

4.3 Influence microdosimetric heterogeneity on tumor control

The shape of the Tumor Control curve is shown in **Figure 16** for a uniform cell line with different radiation modalities as a function of the absorbed dose (upper scale) and approximately normalized to the 50% tumor control dose (≈Dose Equivalent, lower scale) to more clearly see the effect of increasing microscopic heterogeneity as measured by the microdosimetric relative standard deviation (σ_μ) with increasing ion mass, LET and RBE. Not only do the hot spots often in the form of Dual Double Strand Brakes (DDSB's, cf. **Figure 18**, [4: **Figure 2**]) and cold regions get more extreme with increasing LET, but also the RBE is increasing so the reduction of the total dose is about threefold with carbon, neutron, and neon increasing the relative standard deviation and reducing the clinical dose-response slope γ_C severely. A steeper tumor control curve generally increases the therapeutic window of radiation therapy since the absorbed dose distribution and the associated therapeutic effect over the therapeutic window can be modulated with greater efficiency with a

steeper tumor cure and normal tissue damage curves [5]. Also with boron ions the last ≈ 10 GyE should therefore be delivered by low LET beams [5].

4.4 Apoptosis and senescence

Since apoptosis is nature's way to eliminate unwanted cells during the development of practically all organs and is therefore not generally associated with any inflammatory responses accompanying the more common necrotic type of cell kill. In addition, permanent cell cycle arrest or senescence and apoptosis are increasingly induced by light ions. Apoptosis through caspase 3 may cause accelerated tumor cell repopulation after a non-curative treatment [9]. Senescence may therefore be the most desirable endpoint of cancer therapy as the tumor cells lose their reproductive ability and are then slowly disappearing depending on the remaining cellular lifetime or half-life ≈ 2.5 years. As seen in **Figure 18** the tumor was reduced to about half the diameter or 10–15% of the initial volume 6 years after the treatment. Due to the fact that more ions per unit dose and cell kill are needed at medium to low ionization density, the more effective apoptotic and senescent response is obtained at an ionization density of around 20 eV/nm to 40 eV/nm as shown theoretically and experimentally in **Figures 15 and 16** [29]. Interestingly, helium, lithium and boron combine a high local apoptotic and senescent tumor cell inactivation only a few mm around their Bragg peaks and can thus be regarded as the ultimate stereotactic and conformal radiation modality (cf **Figures 1, 7, 12** [29–33]).

5. Conclusions

With boron ions the clinical experience from NIRS (National Institute for Radiological Sciences, Chiba) and other centers in Japan and Germany with carbon is an invaluable asset. A very promising development seen at NIRS is the very effective sterilization of large tumor masses (10–15 cm) such as pelvic chordomas as shown in **Figure 18** [29, 31–35]. These tumors show a gradual disappearance down to 10% and below the initial volume about 5 years after the treatment, probably due to a persistent senescent response likely to be even more effective with boron ions [35], and without evidence of any further tumor growth. The clinical value of light ion beams is discussed in further detail in a number of recent references [2, 5, 10, 19, 20, 29–34, 36]. When the above methods are brought into clinical use a mean tumor cure as high as 80% should be possible, and even more if the new therapeutic dose delivery principles [5], advanced dose fractionation [4: Figure 21, 5], and early tumor detection [10] and malignancy determination methods [37] come into more regular use.

IntechOpen


IntechOpen

Author details

Anders Brahme
Department of Oncology-Pathology, Karolinska Institutet, Stockholm, Sweden

*Address all correspondence to: andersbrah@gmail.com

IntechOpen

© 2023 The Author(s). Licensee IntechOpen. This chapter is distributed under the terms of the Creative Commons Attribution License (<http://creativecommons.org/licenses/by/3.0>), which permits unrestricted use, distribution, and reproduction in any medium, provided the original work is properly cited. 

References

- [1] Brahme A. Quantifying cellular repair, misrepair and apoptosis induced by boron ions, gamma rays and PRIMA-1 using the RHR formulation. *Radiation Research*. 2022;**198**:271-296
- [2] Brahme A, editor. *A Brief Introduction to The Development of Radiation Therapy Optimization*. Ch 1 In: Biologically optimized radiation therapy. Singapore: World Scientific Publishing; 2014:1-15
- [3] Brahme A, Löf J. Fundamentals of physically and biologically based radiation therapy optimization In: Brahme A. editor. *Comprehensive BioMedical Physics*. Vol. 9 Ch 12. Elsevier Oxford: Major Reference Work; 2014. p. 271-313
- [4] Brahme A. A DNA repair-based model of cell survival with important clinical consequences. *Radiation Research*. 2020;**194**:202-235
- [5] Brahme A. On the Ultimate Biological Optimization Steps of Curative Radiation Oncology. *Cancers*, In Press; 2023
- [6] Buscemi G, Perego P, Carenini N, Nakanishi M, Chessa L, Chen J, et al. Activation of ATM and Chk2 kinases in relation to the amount of DNA strand breaks. *Oncogene*. 2004;**23**:7691-7700
- [7] Enns L, Bogen KT, Wizniak J, Murtha AD, Weinfeld M. Low-dose radiation hypersensitivity is associated with p53-dependent apoptosis. *Molecular Cancer Research*. 2004;**2**:557-566
- [8] Short SC, Bourne S, Martindale C, Woodcock M, Jackson SP. DNA damage responses at low radiation doses. *Radiation Research*. 2005;**164**:292-302
- [9] Zhao M, Wang Y, Zhao Y, He S, Zhao R, Song Y, et al. Caspase-3 knockout attenuates radiation-induced tumor repopulation via impairing the ATM/p53/Cox-2/PGE2 pathway in non-small cell lung cancer. *Aging*. 2020;**12**:21758-21776
- [10] Brahme A. High resolution molecular radiation therapy and tumor imaging for the 21st century. *Journal of Nuclear Medicine Radiology & Radiation Therapy*. 2016;**7**:1-311. DOI: 10.4172/2155-9619.1000311+
- [11] Brahme A. Development of Highly Specific Molecular Cancer Therapy with the Lightest Ions. *Book of Abstract Japan: 5th Takahashi Memorial International Symposium*; 2007. p. 57
- [12] Nakamura Y. Isolation of p53-target genes and their functional analysis. *Cancer Science*. 2004;**95**:7-11
- [13] Williams AB, Schumacher B. p53 in the DNA-damage-repair process. *Cold Spring Harbor Perspectives in Medicine*. 2016;**6**:a026070
- [14] Brahme A, Rydberg B, Blomqvist P. Dual spatially correlated nucleosomal double strand breaks in cell inactivation. In: Goodhead DT, O'Neill P, Menzel HG, editors. *Microdosimetry: An Interdisciplinary Approach*. Cambridge, UK: The Royal Society of Chemistry; 1997. pp. 125-128
- [15] Frankenberg D, Frankenberg-Schwager M, Harbich R. The contribution of OH* in densely ionizing electron track ends or particle tracks to the induction of DNA double strand breaks. *Radiation Protection Dosimetry*. 1990;**31**:249-252
- [16] Stenerlöw B, Höglund E, Carlsson J, Blomqvist E. Rejoining of

- DNA fragments produced by radiations of different linear energy transfer. *International Journal of Radiation Biology*. 2000;**76**:549-557
- [17] Ward JF. DNA damage produced by ionizing radiation in mammalian cells: Identities, mechanisms and reparability. *Progress in Nucleic Acid Research and Molecular Biology*. 1988;**35**:95-125
- [18] Brahme A. Accurate description of the cell survival and biological effect at low and high doses and LETs. *Journal of Radiation Research*. 2011;**52**:389-407
- [19] Blakely EA, Chang PY. Biology of charged particles. *Cancer Journal*. 2009;**15**:271-284
- [20] Kempe J, Gudowska I, Brahme A. Depth absorbed dose and *LET* distributions of therapeutic ¹H, ⁴He, ⁷Li and ¹²C beams. *Medical Physics*. 2007;**34**:183-192
- [21] Raju MR. *Heavy Particle Radiotherapy*. London: Academic Press; 1980
- [22] Hall EJ, Wu CS. Radiation-induced second cancers: The impact of 3D-CRT and IMRT. *International Journal of Radiation Oncology, Biology, Physics*. 2003;**56**:83-88
- [23] Brahme A, Ågren AK. On the optimal dose distribution for eradication of heterogeneous tumors. *Acta Oncologica*. 1987;**26**:377-385
- [24] Brahme A, Källman P, Lind BK. Optimization of proton and heavy ion therapy using an adaptive inversion algorithm. *Radiotherapy and Oncology*. 1989;**15**:189-197
- [25] Nardella C, Clohessy JG, Alimonti A, Pandolfi PP. Pro-senescence therapy for cancer treatment. *Nature Reviews. Cancer*. 2011;**11**:503-511
- [26] Gorgoulis V, Adams PD, Alimonti A, Bennett DC, Bishop O, Bishop C, et al. Cellular senescence: Defining a path forward. *Cell*. 2019;**179**:813-827
- [27] Bykov VJN, Eriksson SE, Bianchi J, Wiman KG. Targeting mutant p53 for efficient cancer therapy. *Nature Reviews. Cancer*. 2018;**18**:89-102
- [28] Rubbia C, Ferrari A, Kadi Y, Vlachoudis V. Beam cooling with ionization losses. *Nuclear Instruments and Methods in Physics Research A*. 2006;**568**:475-487
- [29] Vreede P, Brahme A. Development of biologically optimized radiation therapy: Maximizing the apoptotic cell kill. *Radio Science*. 2009;**52**(7):31-52. Available from: <http://www.nirs.go.jp/info/report/rs-sci/pdf/200907.pdf>
- [30] Brahme A, Svensson H. Physical, biological and clinical background for the development of biologically optimized light ion therapy. In: Brahme A, editor. *Biologically Optimized Radiation Therapy*. World Scientific Publishing: Singapore; 2014. pp. 499-648
- [31] Brahme A. Potential developments of light ion therapy The ultimate conformal treatment modality. *Radio Science*. 2009;**52**(2):8-31. Available from: <http://www.nirs.go.jp/info/report/rs-sci/pdf/200902.pdf>
- [32] Brahme A. Optimal use of light ions for radiation therapy. *Radio Science*. 2010;**53**(8-9):35-61. Available from: <http://www.nirs.go.jp/publication/rs-sci/pdf/201008.pdf>
- [33] Imai R, Kamada T, Sugahara S, Tsuji H, Tsujii H. Carbon ion radiotherapy for sacral chordoma. *The British Journal of Radiology*. 2011;**84**:S48-S54

[34] Imai R, Kamada T, Araki N. Carbon ion radiation therapy for unresectable sacral chordoma: An analysis of 188 cases. *International Journal of Radiation Oncology, Biology, Physics*. 2016;**95**:322-327

[35] Kumar S, Suman S, Fornace AJ Jr, Datta K. Space radiation triggers persistent stressresponse, increases senescent signaling, and decreases cell migration in mouse intestine. *Proceedings of the National Academy of Sciences of the United States of America*. 2018;**115**:201807522

[36] Yamada S, Yamamoto N, Koto M, Imai R, Kasuya G, Okonogi N, et al. Current status and perspective of carbon ion radiotherapy. *Radioisotopes*. 2019;**68**:395-402

[37] Rye IH, Lundin P, Måner S, Fjellidal R, Naume B, Wigler M, et al. Quantitative multigene FISH on breast carcinomas. *Gen Chromo Ca*. 2015;**54**:235-248